SAND2013-7836C

Fall Technical Meeting
of the Western States Section of the Combustion Institute
Hosted by Colorado State University
October 7-8, 2013
Paper #13F-65

A Sophisticated Model to Predict Ash Inhibition during Combustion of Pulverized Char Particles

Christopher R. Shaddix and Yanqing Niu[1]

Combustion Research Facility
Sandia National Laboratories
Livermore, CA 94550

Final burnout of char particles from practical fuels such as coal and biomass occurs in the presence of a large ash component. Also, newly utilized coal resources, such as those from India, often contain much larger ash fractions than have traditionally been utilized. Similarly, lignin-rich residues from biochemical processing of biomass often contain high ash fractions and have been shown to burn slowly. In the past, the inhibitory influence of ash on pulverized coal particle combustion has been most frequently modeled using an ash film model, though such films are rarely found when examining partially combusted particles. Conversely, previous EDX probing has suggested that mineral components exposed on the surface of burning pulverized coal particles frequently diffuse back into the char matrix, whose effects can be modeled as an ash dilution effect. To explore the implications of these different ash inhibition models on the temporal evolution of char combustion during burnout, we have developed a new model that considers the possibility of an ash film effect, an ash dilution effect, or some arbitrary combination of the two effects acting in tandem, which is the most realistic scenario. This new model predicts that ash content will have a significant impact on the char burnout rate, and the specific rate is dependent on whether an ash film or ash dilution effect is most prominent. Comparison against experimental data suggests that the ash dilution effect has a larger role than development of an ash film during combustion of pc chars.

1. Introduction

A number of different char burnout models have been constructed over the years for application to fluidized bed or pulverized coal combustors, and some of these have considered the influence of ash on this process [1-5]. Whereas ash effects are unlikely to be very important during the early stages of combustion of low-ash fuels, they become increasingly important during char burnout and can be important throughout the combustion lifetime for higher ash fuels, such as some biomass fuels formed from lignocellulosic ethanol residuals or from certain high-ash coals, such as are common in India [3].

The existing models have all concentrated on using some form of an “ash film” model, whereby the ash that is liberated during the combustion of the carbonaceous matrix accumulates on the

[1] School of Energy and Power Engineering, Xi’an Jiaotong University, Xi’an, China

particle surface and acts to hinder combustion by acting as a diffusional barrier to the transport of oxygen to the encapsulated char core. This model of the influence of ash undoubtedly is a sensible approach when considering fluidized bed combustion, wherein the use of larger fuel particles and moderate conversion temperatures results in significant buildup of ash on the particle surface. However, for pulverized coal particle combustion, the high particle temperatures attained during active char combustion can soften or melt the ash and allow diffusion of liberated ash components back into the char matrix itself [6]. The result of this process on subsequent char combustion is best modeled as an "ash dilution" impact. In fact, experimental investigation of the physical interaction of ash and residual char has found little evidence for the common existence of ash films encapsulating the char [6-9]. In contrast to the prevalent models of ash film inhibition of char combustion in the literature, ash dilution of char combustion has only been formally modeled once [10], where it was demonstrated that this phenomenon can have a dramatic influence on the apparent reaction order when fitting *n*th-order Arrhenius reaction kinetics to experimental data.

During so-called Zone I char combustion, favored by low temperatures and small, unreactive char particles, oxygen penetrates throughout the entire particle and the char burning rate is controlled solely by the chemical reaction and the total surface area available for reaction. During Zone II combustion, which is generally more relevant for pulverized coal combustion conditions, char oxidation is active both in the interior pores of the particle and on the particle surface, with incomplete penetration of oxygen through the particle, such that the burning rate is limited by the combined effects of chemical reaction, available surface area, and oxygen diffusion from the bulk gas to the external char surface and through the porous char. Both for Zone I and Zone II combustion, the char structure, including the surface available for reaction, the porosity, and the presence of mineral or ash constituents within the particle, plays an important role in determining the char oxidation rate. For this reason, there has been a trend in the literature towards the use of intrinsic char kinetics models, which in theory can address these structural effects throughout the oxidation process. Consistent with this trend, we have implemented our ash effects model using a transient intrinsic kinetics approach.

The purpose of this paper is to report on the predictions of a new model of pulverized char particle burnout that treats ash inhibition through either ash film or ash dilution effects, or as some combination of the two. Specifically, the new model allows for allocation of the ash liberated at the particle surface to (a) form an ash film, (b) diffuse back into the particle and participate as a dilution effect, or (c) act as a user-designated fraction of the two effects. In this way, the relative impact of the different modes of ash inhibition can be evaluated, and, by comparing to some experimental data on char combustion and burnout, insight can be achieved into the actual nature of the ash inhibition process during pulverized coal char combustion.

2. Model Description

Fig.1 shows the schematic illustration of the integrated ash model. An initial char particle with a diameter d_0 is divided into N equally spaced concentric shells, and in burning process the particle ideally consist of an external ash layer and an internal char core where ash and carbon are distributed uniformly. It is assumed that X fraction of the ash product in each burned shell thickens the ash layer, and the remaining is penetrated and uniformly distributed into the char core.

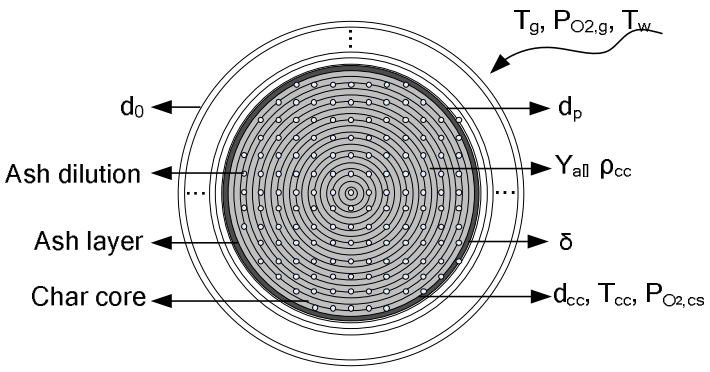

Fig.1 Integrated ash layer and ash dilution model

For simplification of description and treatment, the model is divided into five sub-models: kinetic reaction sub-model, ash layer sub-model, ash dilution sub-model, diffusion sub-model and energy balance sub-model. The reacting char particle is assumed to be spherical and to have uniform properties throughout the particle. Any catalytic effect of the ash constituents is neglected and the ash constituents are assumed to not vaporize.

2.1 Ash layer sub-model

The ash layer sub-model is used to calculate the temporal evolution of the external ash layer thickness, δ. As the char particle burns, a designated fraction X ($0 \le X \le 1$) of the ash products liberated at the surface of the particle is used to form an ash layer. Based on the mass balance equation (Eq.1), the ash layer thickness, δ, can be expressed as Eq.2.

$$X\rho_{cc}\frac{\pi}{6}(d_{cc}^3 - d_{ccc}^3)Y_{a,cc} + m_{al,cc} = \frac{\pi}{6}\rho_{a,f}[(d_{ccc}+2\delta)^3 - d_{ccc}^3] \quad (1)$$

$$2\delta = \left(\frac{X\rho_{cc}(d_{cc}^3 - d_{ccc}^3)Y_{a,cc} + 6m_{al,cc}/\pi}{\rho_{a,f}} + d_{ccc}^3\right)^{\frac{1}{3}} - d_{ccc} \quad (2)$$

where $\rho_{a,f}$ represents the apparent density of ash, which is related to nonporous ash density $\rho_{a,n}$ by Eq.3. $\rho_{a,n}$ is assumed to be $2.65\text{x}10^3$ (kg/m^3) [4], and $\theta_{a,f}$, the ash porosity, is assumed to be 0.25.

$$\rho_{a,f} = \rho_{a,n}(1-\theta_{a,f}) \quad (3)$$

2.2 Ash dilution sub-model

The presence of ash constituents within the char particle changes its porosity, pore size distribution, specific internal surface area, as well as the diffusion resistance of gaseous reactants and products through the char pores [9-12]. The ash dilution sub-model is designed to calculate residual carbon in the char core $m_{c,cc}$, the density of the char core ρ_{cc}, the mass loss Z, etc. Considering the effect of ash and porosity in the char particle, the overall burning rate q_{heat}

consisting of the combination of the internal and external burning rates of the char, is given by Eq.4.

$$q_{heat} = (1 - Y_{a,cc} - \theta_{c,cc} + \frac{\eta \rho_{c,cc} S_g d_{cc}}{6}) q_{c,\text{int}} \quad (4)$$

where $\theta_{c,cc}$ is the porosity of carbon, η is the internal effectiveness factor, S_g is the specific internal surface area of carbon. η is a dimensionless factor is obtained through Eq.5, in which Φ is a generalized Thiele modulus for spheres as shown in Eq.6. According to reference [11], Eq.5 and Eq.6 yield accurate approximations of η for reaction order n from 0 to 1.

$$\eta = \frac{1}{\Phi}[\coth(3\Phi) - \frac{1}{3\Phi}] \quad (5)$$

$$\Phi = \frac{d_{cc}}{6}[\frac{(n+1) k_s S_g \rho_{c,cc} (P_{cs} / RT)^{(n-1)}}{2 D_{\text{eff}}}]^{1/2} \quad (6)$$

Effective diffusivity factor D_{eff} defined in Eq.7 involves the effect of carbon and ash by volume proportion. D is the molecular diffusivity of reactants, σ_c is the constriction factor and τ is the tortuosity. τ/σ_c is assumed to be 6.0 [5]. Eq.8 is which used to calculate the specific internal surface area Sg. S_{g0} and ψ are assumed to have values of 247 m^2/g and 3.0 [12].

$$D_{\text{eff}} = \frac{D \sigma_c}{\tau} (\theta_{a,f} V_{a,cc} / V_{cc} + \theta_c V_{c,cc} / V_{cc}) \quad (7)$$

$$S_g = (\rho_0 / \rho_c) S_{g0} (1 - N)(1 - \psi \ln(1 - N))^{1/2} \quad (8)$$

The carbon burning rate $q_{c,\text{int}}$ per unit external surface of char core is calculated according to the Arrhenius expression as follows:

$$q_{c,\text{int}} = A_{\text{int}} \exp(-E_{\text{int}} / RT_{cc}) P_{cc}^{n_{\text{int}}} \quad (9)$$

2.3 Diffusion sub-model

In Zone II, the char reaction is controlled by both chemical reaction and diffusion. Thus, the reactants content on the surface of the char core P_{cs} and the maximum diffusion rate q_{max} through the ash film need to be calculated. Considering the effects of Stefan flow and ash layer, q_{max} and P_{cs} are deduced from Eq.11 and Eq.12 [4]. k_d, the mass transfer coefficient is calculated according to Eq.13.

$$q_{\max} = \frac{k_d P}{\gamma} \ln[\frac{1}{1 - \gamma P_g / P}] \quad (11)$$

$$P_{O_2,cs} = \frac{P}{\gamma} + \left[P_g - \frac{P}{\gamma} \right] \exp(\frac{q\gamma}{k_d P}) \quad (12)$$

$$k_{\mathrm{d}} = \frac{ShDd_{\mathrm{p}}\theta_{a,f}^{2.5}M_{\mathrm{c}}}{RT_{\mathrm{m}}\nu(Sh\delta d_{\mathrm{c}} + \theta_{a,f}^{2.5}d_{\mathrm{c}}^{2})} \qquad (13)$$

2.4 Heating balance sub-model

The char core temperature T_{cc} and particle temperature T_{p} are computed through Eq.14-18, which considers the radiation heat transfer, convection heat transfer and conductive heat transfer. The heat released through char oxidation in the char core is transferred to the ash layer through conduction, and then through convection and radiation to the surroundings. The thermal conductivity coefficient of the ash layer in Eq.19 is given by reference [13].

$$Q_{rxn} = Q_{cond} = Q_{conv} + Q_{rad,p} \quad (14)$$

$$Q_{rxn} = [q_{\mathrm{O2,\,rxn}}(FCO_2\Delta H_{\mathrm{CO_2}} + (1-FCO_2)\Delta H_{\mathrm{CO}}) + q_{\mathrm{H2O,\,rxn}}\Delta H_{\mathrm{H2O}}]A_{cc} \quad (15)$$

$$Q_{cond} = \pi d_p d_{cc}\lambda_a(T_{cc} - T_p)/\delta \quad (16)$$

$$Q_{conv} = h(T_p - T_g)A_p \quad (17)$$

$$Q_{rad,p} = \sigma\varepsilon(T_p^4 - T_w^4)A_p \quad (18)$$

$$\lambda_a = 0.0015T_p^{1.1} \quad (19)$$

3. Results and discussion

3.1 Comparison of predictions against experimentally measured T_{p} and N

Fig.2 shows a comparison of particle burning temperatures and carbon conversion rates for experimental measurements and predicted values when ignoring the effect of gasification reactions. It can be seen that without the influence of gasification reactions, the char particle combustion temperature increases more rapidly with increases in ambient oxygen concentration than experimentally measured. This is consistent with the results found by Hecht et al. [14,15], wherein the endothermic effect of gasification reactions moderates the char combustion temperature, particularly for combustion in elevated oxygen contents. Meanwhile, the predicted carbon conversion rates all compare well to the experimental data. This result is also consistent with the expected minor influence of gasification reactions on the predicted char burning rate. Hecht et al. found that the overall effect of the combined steam and CO_2 gasification reactions is

to increase the carbon conversion rate by approximately 10% in typical oxy-fuel combustion environments[15]. Overall, the predicted trends are fairly insensitive to the assumed intrinsic char kinetic reaction order. For subsequent calculations, an oxidation reaction order of 0.1 is used.

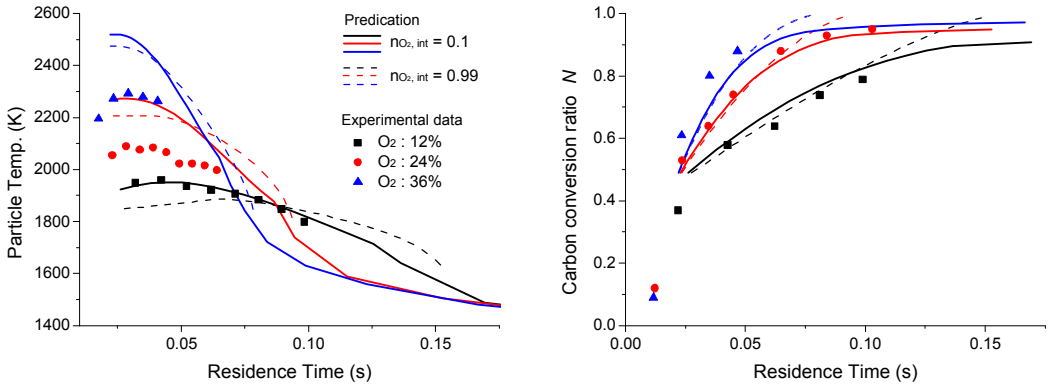

Fig.2 Predicted and measured average temperatures and carbon conversion rate of the eastern bituminous char particle for three O_2 concentrations, 14 vol% moisture, and N_2 bath gas. Symbols: Experimentally measured data [16]; Line: Predicted data. Initial char diameter: 115μm ; Initial ash content: 26.3 wt%; Wall temperature: 500K; XX = 0.16; $A_{O2,\ int}$=8000 g·s·cm^{-2}·atm^{n}; $E_{O2,\ int}$=150 kJ/mol; without steam gasification reaction.

Fig.3 shows a comparison of particle burning temperatures and carbon conversion rate between experimentally measured data and predicated data taking into account both the oxidation reaction and the steam gasification reaction. It can be seen that the predicted values from combined oxidation and steam gasification reactions are very close to the experimental measurements.

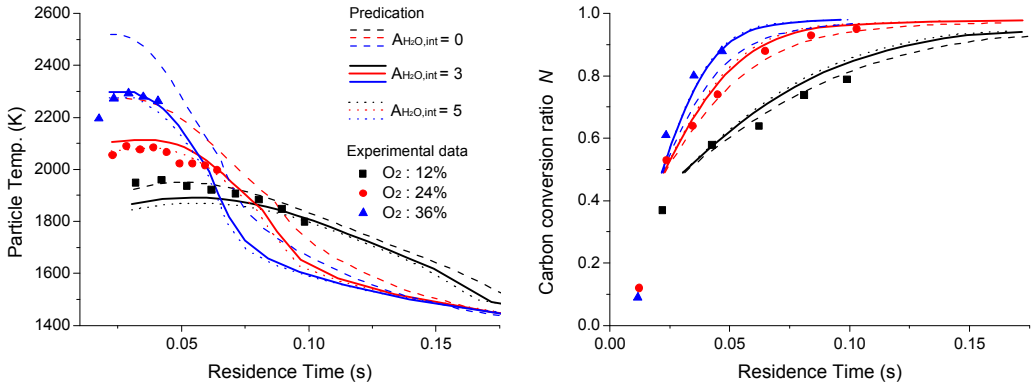

Fig.3 Same as for Fig. 2, with $A_{O2,\ int}$=8000 g·s·cm^{-2}·atm^{n}; $E_{O2,\ int}$=150 kJ/mol; $n_{O2,\ int}$: 0.1; $E_{H2O,\ int}$: 222 kJ/mol; $n_{H2O,\ int}$: 0.5.

3.2.3 Ash film vs. ash dilution effects

The effects of ash film and ash dilution on char burning are illustrated in Fig.4. It can be seen that with an increasing fraction of the liberated ash forming an ash film, the char particle temperature decreases, and the char burnout time increases. However, when ignoring the effect of ash film on reactants diffusion, char particle temperature increases and burnout time decreases. $t_{80,\text{ without reactants diffusion}} = 1/2\ t_{80,\text{ with reactants diffusion}}$; $t_{95,\text{ without reactants diffusion}} = 1/3\ t_{95,\text{ with reactants diffusion}}$; $t_{99,\text{ without reactants diffusion}} = 1/4\ t_{99,\text{ with reactants diffusion}}$. Meanwhile, it can be seen form Fig.6b that the burnout time when only a small fraction (0.25) of the liberated ash contributes to an ash film is only slightly lower than that with a larger ash film (and less internal ash dilution). On the other hand, Fig. 6a indicates that the formation of a significant ash film has a fairly dramatic influence on the char particle combustion temperature. In this way, measurements of the time history of char particle temperatures during burnout can give insight into the fraction of liberated ash that contributes to forming an ash film. Based on the data shown in Fig. 2, it appears that the fraction of liberated ash contributing to an external ash film is significantly less than 75%, and is probably less than 50%. These results clearly show the necessity of considering the ash dilution effect of ash constituents embedded in the char particle, and the contribution of liberated ash to that ash dilution effect.

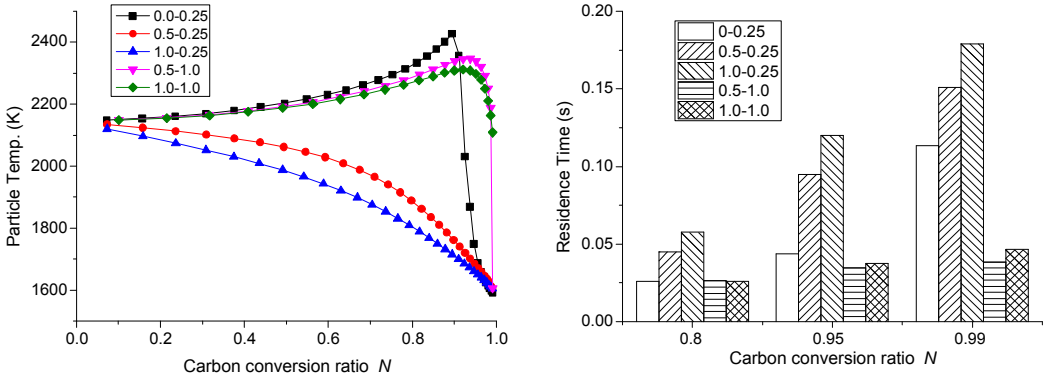

Fig.6 The comparison of the effect of ash film and ash dilution on char burning. Initial char diameter: 100μm ; Initial ash content: 20 wt%; 24 vol% O_2, 14 vol% moisture, 58 vol%N_2 and 4 vol% CO_2; Gas temp. = 1600K; Wall temp. = 500K; $A_{O2,\text{ int}}$ = 8000 g·s·cm^{-2}·atm^{n}; $E_{O2,\text{ int}}$ = 150 kJ/mol; $n_{O2,\text{ int}}$: 0.1; $A_{H2O,\text{ int}}$ = 3 g·s·cm^{-2}·atm^{n};$E_{H2O,\text{ int}}$ = 222 kJ/mol; $n_{H2O,\text{ int}}$ = 0.5. In the legend, the first number is the fraction of the nominal ash content that is considered in the simulation run and the second number is the fraction of the liberated ash that contributes to internal ash dilution (i.e. does not contribute to the external ash film).

3. Conclusions

A new intrinsic kinetics model for the transient combustion of pulverized coal char particles has been developed that allows the interrogation of ash dilution versus ash film inhibition of char burnout. The model kinetics were calibrated against char particle temperature measurements for size-classified high-volatile bituminous coal char particles burning in environments with different oxygen content. This exercise revealed the need to include a steam gasification reaction, together with char oxidation, in order to give good agreement with the measured data trends. Exercising the new model demonstrated the expected dependence of ash influence as a function of the initial char ash content and the extent of burnout. A strong sensitivity of the char combustion temperature trend during burnout was also found, as a function of the extent of liberated ash contribution to the formation of an external ash film. In contrast to the widespread assumption of liberated ash forming an external film, the results suggest that the majority of the liberated ash contributes instead to ash dilution type of effect.

Acknowledgements

Research funding, provided by the China Scholarship Council Postgraduate Scholarship Program and the Department of Energy (DOE) Fossil Energy Cross-Cutting Research Program, managed by Bob Romanosky of NETL, is gratefully acknowledged. Sandia National Laboratories is a multi-program laboratory managed and operated by Sandia Corporation, a wholly owned subsidiary of Lockheed Martin Corporation, for the U.S. Department of Energy's National Nuclear Security Administration under contract DE-AC04-94AL85000.

References

[1] C. Chen, T. Kojima, Fuel Processing Technology 47 (1996) 215-232.

[2] H. T. Zhang, J. H. Yan, M. J. Ni, K. F. Cen, Combustion Science and Technology 174 (2002) 55-73.

[3] S. Jayanti, K. Maheswaran, V. Saravanan, Applied Mathematical Modelling 31 (2007) 934-953.

[4] R. Hurt, J.-K. Sun, M. Lunden, Combust. Flame 113 (1998) 181-197.

[5] J.-K. Sun, R.H. Hurt, Proc. Combust. Inst. 28 (2000) 2205–2213.

[6] M.M. Lunden, N.Y.C. Yang, T.J. Headley, C.R. Shaddix, Proc. Combust. Inst. 27 (1998) 1695–1702.

[7] R.H. Hurt, K.A. Davis, Proc. Combust. Inst. 25 (1994) 561–568.

[8] R.H. Hurt, K.A. Davis, N.Y.C. Yang, D. Hardesty, “The Origin and Properties of Unburned Carbon from Pulverized-Coal Combustion,” EPRI technical report, EPRI TR-105743, Nov. 1995.

[9] R.H. Hurt, K.A. Davis, Combust. Flame 116 (1999) 662-670.

[10] J.J. Murphy, C.R. Shaddix, Combust. Flame 157 (2010) 535-539.

[11] D.R. Froment, K.B. Bischoff, Chemical reactor analysis and design, John Wiley and Sons, New York, 1990, p. 162.

[12] R.E. Mitchell, L.Q. Ma, B. Kim, Combustion and Flame 151 (2007) 426-436.

[13] H. R. Rezaei; R. P. Gupta; G. W. Bryant; J. T. Hart; G. S. Liu; C. W. Bailey; T. F. Wall; S. Miyamae; K. Makino; Y. Endo, Fuel 79 (13) (2000) 1697-1710.

[14] E.S. Hecht, C.R. Shaddix, A. Molina, B.S. Haynes, Proc. Combust. Instit. 33 (2011) 1699-1706.

[15] E.S. Hecht, C.R. Shaddix, M. Geier, A. Molina, B.S. Haynes, Combust. Flame 159 (2012) 3437-3447.

[16] J.J. Murphy, C.R. Shaddix, Combust. Flame 144 (2006) 710-729.